Inorganic Chemistry

Article

pubs.acs.org/IC

Single-Crystal-to-Single-Crystal Metalation of a Metal–Organic Framework: A Route toward Structurally Well-Defined Catalysts

Miguel I. Gonzalez,[†] Eric D. Bloch,[†] Jarad A. Mason,[†] Simon J. Teat,[‡] and Jeffrey R. Long*[,†,§]

[†]Department of Chemistry, University of California, Berkeley, California 94720, United States

[‡]Advanced Light Source, Lawrence Berkeley National Laboratory, Berkeley, California 94720, United States

[§]Materials Sciences Division, Lawrence Berkeley National Laboratory, Berkeley, California 94720, United States

Supporting Information

ABSTRACT: Metal–organic frameworks featuring ligands with open chelating groups are versatile platforms for the preparation of a diverse set of heterogeneous catalysts through postsynthetic metalation. The crystalline nature of these materials allows them to be characterized via X-ray diffraction, which provides valuable insight into the structure of the metal sites that facilitate catalysis. A highly porous and thermally robust zirconium-based metal–organic framework, $Zr_6O_4(OH)_4(bpydc)_6$ ($bpydc^{2-}$ = 2,2′-bipyridine-5,5′-dicarboxylate), bears open bipyridine sites that readily react with a variety of solution- and gas-phase metal sources to form the corresponding metalated frameworks. Remarkably, $Zr_6O_4(OH)_4(bpydc)_6$ undergoes a single-crystal-to-single-crystal transformation upon metalation that involves a change in space group from $Fm\bar{3}m$ to $Pa\bar{3}$. This structural transformation leads to an ordering of the metalated linkers within the framework, allowing structural characterization of the resulting metal complexes. Furthermore, $Zr_6O_4(OH)_4(bpydc)_6$ yields an active heterogeneous catalyst for arene C–H borylation when metalated with $[Ir(COD)_2]BF_4$ (COD = 1,5-cyclooctadiene). These results highlight the unique potential of metal–organic frameworks as a class of heterogeneous catalysts that allow unparalleled structural characterization and control over their active sites.

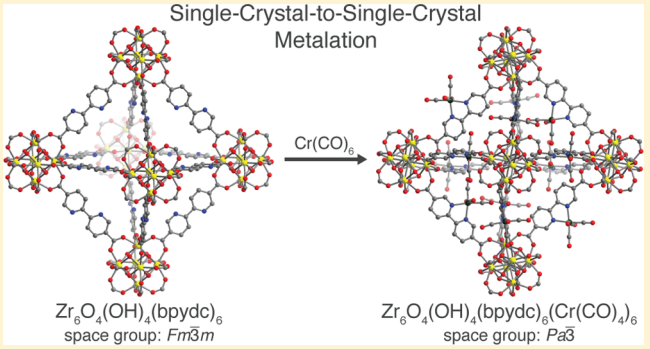

INTRODUCTION

The synthesis of catalysts with highly tunable and well-defined active sites remains an enduring goal in the field of heterogeneous catalysis, as the development of new catalysts has been largely limited by the structural ambiguity and nonuniformity in typical heterogeneous catalysts.[1,2] Although molecular catalysts exhibit tremendous advantages in the ability to design and characterize their active sites, approximately 80% of catalytic processes still adopt heterogeneous systems.[3] This strong industrial preference for heterogeneous catalysts arises from their inherent stability and ease of recovery, which allows more efficient catalyst separation and reuse. Significant advances in preparing and characterizing heterogeneous catalysts with distinct site-isolated active species have been achieved by grafting molecular catalysts onto solid supports coupled with characterization via a comprehensive array of spectroscopic techniques.[1,2] Molecular systems, however, still maintain a considerably higher degree of structural control and are typically more amenable to characterization than heterogeneous materials. In particular, the ability to systematically change the ligand environment of the catalytically active metal site and determine molecular structure by X-ray diffraction remains unrealized in these supported catalysts.

Metal–organic frameworks exhibit the exceptional capability of adopting crystalline structures with both high porosity[4] and specific pore environments,[5,6] resulting in their extensive evaluation for applications in gas storage and gas separation.[7−10] As readily functionalized porous structures, these materials are uniquely suited to combine the structural control available to homogeneous molecular catalysts with the inherent ease of separation and reuse of heterogeneous catalysts. Similar to molecular catalysts, metal–organic frameworks can be easily tailored to give optimal catalytic activity and selectivity.[11−13] Moreover, active site isolation within a solid framework can impart stability to reactive species by preventing intermolecular decomposition pathways, allowing their characterization and use for productive chemistry.[14−18] Finally, the ability to determine the structures of these frameworks through X-ray diffraction enables facile correlation of structure to catalytic activity.[14,19] Altogether, these distinct advantages open up a promising avenue toward the design of robust catalysts with isolated and well-defined active sites.

Much of the research on metal–organic framework catalysis has focused on reactions facilitated by the metal nodes.[14,20−23]

Received: January 13, 2015
Published: February 26, 2015

DOI: 10.1021/acs.inorgchem.5b00096
Inorg. Chem. 2015, 54, 2995−3005

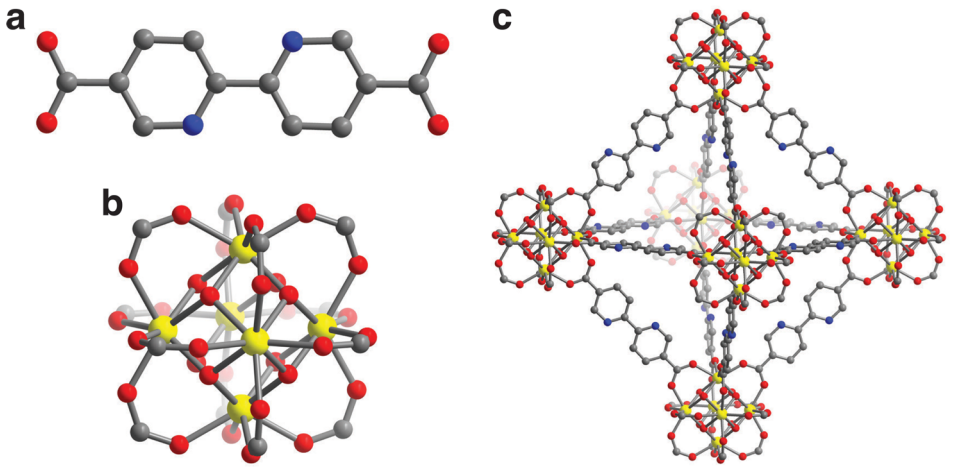

Figure 1. Structure of $bpydc^{2-}$ linkers (a) and the octahedral Zr_6 inorganic nodes (b) in **1**. A portion of the crystal structure of **1** (c) as determined by analysis of single-crystal X-ray diffraction data. The bipyridine nitrogen atoms were found to be disordered over two positions in the crystal structure, but are represented here in specific positions. Yellow, red, blue, and gray spheres represent Zr, O, N, and C atoms, respectively; H atoms are omitted for clarity.

In comparison to molecular catalysts, however, achieving tunability in these systems has been challenging, as only a few metal and linker combinations lead to frameworks with metal sites that are accessible for catalysis. This limits the range of metal sites and coordination environments available to evaluate as potential catalytically active sites. To overcome these limitations, alternative strategies have been developed to allow greater opportunity for catalyst design, such as the encapsulation of catalytically active metal species[24−26] and the use of functionalized linkers to build catalysts into the framework.[13,17,27−30] Among these methods, postsynthetic metalation has emerged as a versatile way to produce materials with isolated and well-defined catalytically active sites.[31−37]

In analogy to how a single ligand family is used to make a diverse set of molecular catalysts, we envisioned using a metal−organic framework with bridging linkers featuring accessible chelating sites as a platform to synthesize catalysts for a variety of reactions. Through judicious choice of the metal source used for postsynthetic metalation, one could potentially prepare a wide range of catalytically active species based not only on the identity of the metal cation but also on the coordinated ancillary ligands.

The synthesis of metal−organic frameworks with open chelating sites requires a strategy that prevents metalation of the chelating site during framework synthesis. This has previously been achieved by using a linker with hard carboxylate donors and a softer chelating moiety, allowing selective metal coordination based on their hard/soft acid properties.[19,38] The hard carboxylate groups preferentially bind to hard oxophilic metal ions to form a porous framework, while the chelating sites remain available for postsynthetic metalation. Metal−organic frameworks derived from $Zr_6O_4(OH)_4(bpdc)_6$ ($bpdc^{2-}$ = biphenyl-4,4′-dicarboxylate) or UiO-67[39] represent ideal systems for this strategy due to their inherent thermal and chemical stability and the strong preference of Zr^{IV} for hard oxygen donors. We anticipated that $Zr_6O_4(OH)_4(bpydc)_6$ ($bpydc^{2-}$ = and 2,2′-bipyridine-5,5′-dicarboxylate), the bipyridine analog of $Zr_6O_4(OH)_4(bpdc)_6$, could be synthesized and employed as a platform for building an array of heterogeneous catalysts through postsynthetic metalation (Figure 1). Indeed, while this Article was in preparation, recent reports have demonstrated the synthesis of this compound and its application in gas separation,[40] H_2S removal,[41] and catalysis.[32,33]

In addition to being a versatile route toward new heterogeneous catalysts, the structural determination of the resulting metalated frameworks can provide insight that is critical to both understanding the mechanism of catalysis and precise tuning of catalyst structure to obtain ideal activity and selectivity. This would demonstrate the ability to characterize and tailor a heterogeneous catalyst to a degree previously only possible for molecular systems. In practice, however, it can be very challenging to determine the structures of the metal−linker complexes formed from postsynthetic metalation, because the high symmetry of most metal−organic frameworks leads to disorder of these sites.[18,30,34,42] Recent work, however, has shown that structurally ordered metal−linker complexes can be achieved if a metal−organic framework has sufficiently low symmetry.[19]

Herein, we report the synthesis of $Zr_6O_4(OH)_4(bpydc)_6$ (**1**) and its subsequent metalation with solution- and gas-phase metal precursors. We demonstrate the unprecedented single-crystal-to-single-crystal metalation of **1** and characterization of the resulting metalated frameworks, **1**·$(CuCl_2)_{5.8}$, **1**·$(CuCl)_{6.8}$, **1**·$(CoCl_2)_{5.5}$, **1**·$(FeBr_2)_{6.1}$, and **1**·$(Cr(CO)_4)_{5.6}$, by single-crystal X-ray diffraction. Remarkably, metalation of the framework leads to a structural transition to a lower symmetry space group, allowing the structural characterization of the metal-bipyridine complexes within the pores. Furthermore, **1** shows catalytic activity in arene C−H borylation upon metalation with $[Ir(COD)_2]BF_4$. These results highlight the unique potential of metal−organic frameworks as heterogeneous catalysts with well-defined site-isolated active sites that can be precisely characterized structurally.

EXPERIMENTAL SECTION

Materials and Methods. All manipulations were performed under an N_2 atmosphere in a VAC Atmospheres glovebox or using standard Schlenk techniques. Acetonitrile, benzene, toluene, hexanes, diethyl ether, and 1,2-difluorobenzene were deoxygenated by purging with argon for 1 h and dried using a commercial solvent purification system designed by JC Meyer Solvent Systems. The compounds 1,3-dimethylbenzene and 1,3-dimethoxybenezne were purchased from Sigma-Aldrich, dried over Na/benzophenone, and degassed via three

DOI: 10.1021/acs.inorgchem.5b00096
Inorg. Chem. 2015, 54, 2995−3005

successive freeze−pump−thaw cycles. Bis(pinacolato)diboron was purchased from Strem and purified by recrystallization from hexanes followed by sublimation at 80 °C and 60 mTorr. The compounds 2,2′-bipyridine-5,5′-dicarboxylic acid (H_2bpydc) and dimethyl [2,2′-bipyridine]-5,5′-dicarboxylate (dmbpydc) were synthesized using a previously published procedure.[29] The compounds $ZrCl_4$, 5,5′-dimethyl-2,2′-bipyridine, 1,3,5-trimethoxybenzene, triphenyl-phosphine (PPh_3), and tricyclohexylphosphine (PCy_3) were purchased from Sigma-Aldrich and used as received. The compounds [Ir(COD)$_2$]BF_4, $FeBr_2$, $CoCl_2$, CuCl, and $CuCl_2$ were purchased from Strem and used as received. All other chemicals were purchased from commercial vendors and used as received unless otherwise noted.

Thermogravimetric analyses were carried out with a TA Instruments TGA Q5000 operating at a ramp rate of 1 °C/min under a 25 mL/min N_2 flow. Air-sensitive samples were prepared as a slurry in hexanes to temporarily protect the sample from oxygen and moisture and quickly loaded into the instrument. Samples were then heated to 100 °C at a rate of 1 °C/min and held at that temperature for 1 h to evaporate the hexanes prior to analysis. Infrared spectra were collected on a PerkinElmer Avatar Spectrum 400 FTIR spectrophotometer equipped with a Pike attenuated total reflectance accessory (ATR) accessory. UV−vis spectra were recorded on a Cary 5000 spectrophotometer equipped with a reflectance sphere for diffuse reflectance spectra. Scanning electron microscopy (SEM) samples were prepared by dispersing crystals in dichloromethane and drop casting onto a silicon chip. In order to dissipate charge, the samples were sputter coated with ∼3 nm of Au (Denton Vacuum, LLC). Crystals were imaged at 5 keV/12 μA by field emission SEM (JEOL FSM6430). Elemental analyses were obtained from the Microanalytical Laboratory of the University of California, Berkeley, using a PerkinElmer 2400 series II combustion analyzer. NMR spectra were acquired on Bruker AVB-400 and AVQ-400 instruments at the University of California, Berkeley, NMR facility. All chemical shifts are given in relation to residual solvent peaks or tetramethylsilane. NMR yields were determined by ^{1}H NMR spectroscopy with 1,3,5-trimethoxybenzene as an internal standard.

$Zr_6O_4(OH)_4$(bpydc)$_6$ (1). H_2bpydc (3.09 g, 12.5 mmol) and benzoic acid (125 g, 1000 mmol), and *N*,*N*-dimethylformamide (DMF; 1 L) from a newly opened bottle, were placed into a three-neck 2-L round-bottom flask equipped with a Schlenk adapter, glass stoppers, and a magnetic stir bar, and the resulting mixture was purged with dry nitrogen for 30 min. Solid $ZrCl_4$ (2.96 g, 12.5 mmol) was then added, and the mixture was purged with dry nitrogen for an additional 30 min. Deionized water (410 μL, 22.8 mmol) was then added, and the mixture was heated with magnetic stirring for 5 days at 120 °C under a nitrogen atmosphere. After allowing the mixture to cool to room temperature, the solvent was decanted, and the resulting white microcrystalline powder was washed by soaking three times in 500 mL aliquots fresh DMF for 24 h at 120 °C, followed by solvent exchange with tetrahydrofuran (THF) via Soxhlet extraction for 3 days. The THF solvated powder was filtered under dry N_2, followed by heating at 120 °C under dynamic vacuum for 24 h to give fully desolvated $Zr_6O_4(OH)_4$(bpydc)$_6$. Yield: 3.70 g, 82%. Anal. Calcd for $C_{72}H_{36}N_{12}O_{32}Zr_6$: C, 40.55; H, 1.98; N, 7.88. Found: C, 41.72; H, 1.98; N, 7.52. IR (solid-ATR): 3205 (br, w), 1653 (m), 1591 (s), 1536 (m), 1403 (s), 1167 (w), 1014 (w), 839 (2), 802 (w), 770 (s), 720 (w), 653 (s), 455 (s).

Single Crystals of $Zr_6O_4(OH)_4$(bpydc)$_6$ (1). H_2bpydc (247 mg, 1.00 mmol), benzoic acid (9.89 g, 80.0 mmol), and anhydrous DMF (80 mL) were placed into a 100 mL Teflon-capped jar and sonicated for 1 min. Solid $ZrCl_4$ (466 mg, 2.00 mmol) was then added, and the mixture was sonicated for 1 min. Deionized water (128 μL) was added, and the mixture was placed in an oven that was preheated to 120 °C, and the vessel was kept at that temperature for 5 days, yielding colorless octahedron-shaped single crystals on the walls of the jar. The crystals were soaked three times in fresh DMF for 24 h at 120 °C, followed by soaking three times in dry deoxygenated THF for 24 h at 70 °C in a Schlenk flask under N_2 atmosphere. The crystals were then kept in THF and stored in a glovebox under N_2 atmosphere. Characterization of the crystals was performed using single-crystal X-ray diffraction.

General Procedure for Metalation of 1 with Solution-Phase Metal Precursors. Microcrystalline **1** (50−500 mg), the desired metal source (0.10−1.0 equiv per bpydc), and acetonitrile (3 mL) were mixed in a 20 mL Teflon-capped vial. The resulting mixture was then heated for a week on a hot plate at 80 °C to afford a colored powder. After cooling to room temperature, the solvent was decanted, and the powder was soaked three times in fresh acetonitrile for 24 h at 80 °C in order to remove any unreacted metal source. The solvent was then removed under reduced pressure at 80 °C to give the corresponding metalated framework. Metal insertion reduces the stability of the framework to moisture. Thus, metalation and subsequent manipulations were carried out under an inert atmosphere.

Single crystals of **1** in THF were placed in a 4 mL Teflon-capped vial. Most of the solvent was pipetted out, followed by addition of excess (10−20 mg) metal source in acetonitrile. The mixture was allowed to react for 7 days at 80 °C, resulting in a color change of the crystals. Most of the solution was removed by pipet, and the crystals were subsequently soaked three times in fresh acetonitrile at 80 °C for 24 h, and were then used for single-crystal X-ray diffraction experiments.

Metalation of 1 with $Cr(CO)_6$. Microcrystalline powder of $Zr_6O_4(OH)_4$(bpydc)$_6$ (10−50 mg) in a 4 mL vial was placed in a 20 mL vial containing excess $Cr(CO)_6$. The 20 mL vial was sealed with a Teflon cap and heated for 7 days at 80 °C. The resulting dark green solid was washed three times with benzene at 80 °C to remove any unreacted $Cr(CO)_6$, and was then heated at 80 °C under reduced pressure for 24 h to give **1**·$(Cr(CO)_4)_{5.6}$.

Single crystals of $Zr_6O_4(OH)_4$(bpydc)$_6$ in THF or benzene were placed in a 4 mL Teflon-capped vial. Most of the solvent was pipetted out, and the 4 mL vial was placed within a 20 mL vial containing excess $Cr(CO)_6$. The 20 mL vial was sealed with a Teflon cap and heated for 7 days at 80 °C. The resulting dark green crystals were either used directly or soaked in acetonitrile then used for single-crystal X-ray diffraction experiments.

$Zr_6O_4(OH)_4$(bpdc)$_6$ (2). This material was synthesized by substituting H_2bpydc with H_2bpdc in the synthetic procedure for **1** above. Anal. Calcd for $C_{84}H_{52}O_{32}Zr_6$: C, 47.58; H, 2.47; N, 0. Found: C, 47.85; H, 2.11; N, 0.

[Ir(dmbpydc)(COD)]BF_4 (3). In a 20 mL vial, dmbpydc (22.0 mg, 0.0808 mmol) was added to a solution of [Ir(COD)$_2$]BF_4 (40.2 mg, 0.0811 mmol) in acetonitrile (3 mL). The initially yellow solution immediately turned dark green upon addition of dmbpydc. The vial was sealed with a Teflon cap and allowed to stir at room temperature for 12 h. The resulting dark green solution was then concentrated under reduced pressure. Layering or slow diffusion of diethyl ether over the concentrated solution afforded dark green crystals, which were suitable for single-crystal X-ray analysis. After carefully decanting the solvent, the crystals were washed with diethyl ether and dried under reduced pressure to give [Ir(dmbpydc)(COD)]BF_4. Yield: 38.2 mg, 72%. Anal. Calcd for $C_{22}H_{24}BF_4IrN_2O_4$: C, 40.07; H, 3.67; N, 4.25. Found: C, 39.62; H, 3.40; N, 4.72. ^{1}H NMR (400 MHz, CD_3CN) δ 8.778 (dd, 2H), 8.703 (d, 2H), 8.537 (d, 2H), 4.406 (m, 4H), 3.971 (s, 6H), 2.405 (m, 4H), 2.035 (m, 4H). IR (solid-ATR): 3121 (w), 3067 (w), 3000 (w), 2958 (w), 2894 (w), 2841 (w), 1721 (m), 1611 (2), 1427 (w), 1296 (m), 1276 (m), 1191 (w), 1128 (m), 1027 (br, m), 867 (w), 760 (m), 523 (w), 484 (w).

RESULTS AND DISCUSSION

Synthesis of $Zr_6O_4(OH)_4$(bpydc)$_6$. Reaction of $ZrCl_4$ with H_2bpydc in the presence of 80 equiv of benzoic acid and 1.8 equiv of water in DMF at 120 °C for 5 days affords **1** as a white microcrystalline solid. Powder X-ray diffraction data show that **1** is isostructural to $Zr_6O_4(OH)_4$(bpdc)$_6$ (Supporting Information Figure S8). Thermogravimetric analysis data collected for the as-synthesized material (Supporting Information Figure S32) shows a 41% mass loss from 40 to 120 °C, which is

DOI: 10.1021/acs.inorgchem.5b00096
Inorg. Chem. 2015, 54, 2995−3005

Table 1. Selected Properties of the Metal–Organic Frameworks Presented in this Work

compd	color	metal loading[a] (%)	SA_{Lang}[b] (m^2/g)	SA_{BET}[c] (m^2/g)
1	white		2772	2730
2	white		2805	2625
1·$(CuCl_2)_{5.8}$	green	96(1)	1253	1101
1·$(CuCl)_{6.8}$	light brown	114(3)	835	701
1·$(CoCl_2)_{5.5}$	pale blue	92(1)	1282	1204
1·$(FeBr_2)_{6.1}$	red-violet	101.1(7)	1073	971
1·$(Cr(CO)_4)_{5.6}$	dark green	93(2)	1065	934

[a]Metal loading was determined by ICP-OES based on the molar ratio of the inserted metal relative to Zr in the framework. [b]SA_{Lang} = Langmuir surface area. [c]SA_{BET} = Brunauer–Emmett–Teller (BET) surface area.

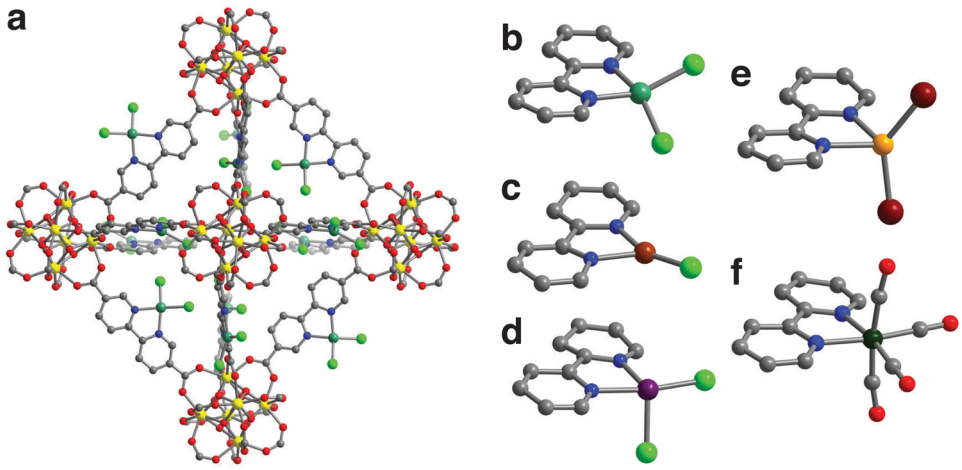

Figure 2. Portion of the crystal structure of **1**·$(CuCl_2)_{5.8}$ (a) as determined by analysis of single-crystal X-ray diffraction data. Structures of the bipyridine metal complexes in **1**·$(CuCl_2)_{5.8}$ (b), **1**·$(CuCl)_{6.8}$ (c), **1**·$(CoCl_2)_{5.5}$ (d), **1**·$(FeBr_2)_{6.1}$ (e), and **1**·$(Cr(CO)_4)_{5.6}$ (f), as determined from single-crystal X-ray diffraction data. Yellow, green, brown, purple, light orange, dark green, light green, dark red, red, blue, and gray spheres represent Zr^{IV}, Cu^{II}, Cu^{I}, Co^{II}, Fe^{II}, Cr^{0}, Cl, Br, O, N, and C atoms, respectively; H atoms and acetonitrile molecules in the pores are omitted for clarity. Note that 53% of the Cu-bipyridine complexes in **1**·$(CuCl)_{6.8}$ were found to have $[CuCl_2]^-$ as a counteranion instead of Cl^- (Supporting Information Figure S1), while the bipyridine complexes in **1**·$(CoCl_2)_{5.5}$ and **1**·$(FeBr_2)_{6.1}$ exist in different coordination geometries due to different degrees of solvation (Supporting Information Figures S2–S3). The coordinated solvent molecules in **1**·$(CoCl_2)_{5.5}$ and **1**·$(FeBr_2)_{6.1}$ could not be modeled due to disorder and weak scattering of the solvent molecules in comparison to the halide ligands.

associated with framework desolvation. No further mass loss is observed until the framework decomposes at temperatures above 450 °C, which suggests that **1** has comparable thermal stability to $Zr_6O_4(OH)_4(bpdc)_6$.[39,43] The fully desolvated material exhibits Langmuir and BET surface areas of 2772 and 2730 m^2/g, respectively, which are close to 3000 m^2/g, the reported Langmuir surface area of $Zr_6O_4(OH)_4(bpdc)_6$.[39] SEM images of the bulk powder sample of **1** (Supporting Information Figure S39) reveal that the material forms well-faceted octahedron-shaped crystals roughly 0.5–1 μm on an edge.

Benzoic acid is critical to the synthesis of highly crystalline **1**. Attempts to synthesize it in the absence of benzoic acid result in powders with poor crystallinity. Powder X-ray diffraction analysis reveals that increasing the amount of benzoic acid (0–80 equiv per linker) leads to more crystalline material (Supporting Information Figure S10), which is in agreement with results reported in a similar study for $Zr_6O_4(OH)_4(bpdc)_6$.[43] This effect is thought to arise from competition between benzoic acid and the dicarboxylic acid linkers during framework assembly, making framework formation more reversible.[43] In addition, having more benzoic acid present in the reaction mixture also requires longer reaction times. As an example, precipitate formation can be observed within a few hours if no benzoic acid is added, while it takes 2–3 days for the solid product to be observed in the presence of 80 equiv of benzoic acid per linker. Attempts to synthesize the material with the addition of 100 or greater equivalents of benzoic acid per linker yielded no observable precipitate over 5 days.

The synthesis of X-ray quality single crystals of **1** required more careful control of the reaction conditions. In particular, both the amount of water added and the metal-to-ligand ratio had significant effects on the size and quality of the crystals. Though highly crystalline and porous **1** can be reproducibly synthesized using commercially available DMF, reproducible formation of single crystals requires the addition of a precise amount of water to anhydrous DMF obtained from a solvent purification system. Reaction conditions that use anhydrous DMF alone fail to yield any precipitate, which is consistent with the requirement of water to form the μ_3-O and μ_3-OH groups of the Zr_6 octahedral nodes.[43] Interestingly, the addition of 2 equiv of $ZrCl_4$ per linker yields isolated and regularly shaped octahedral crystals. In contrast, conditions that employ stoichiometric amounts of $ZrCl_4$ per linker produce crystals that are intergrown.

X-ray analysis of an as-synthesized single crystal of **1** further confirmed that the framework is isostructural to $Zr_6O_4(OH)_4(bpdc)_6$ (Figure 1). The calculated powder diffraction pattern obtained from the crystal structure agrees well with the

DOI: 10.1021/acs.inorgchem.5b00096
Inorg. Chem. 2015, 54, 2995–3005

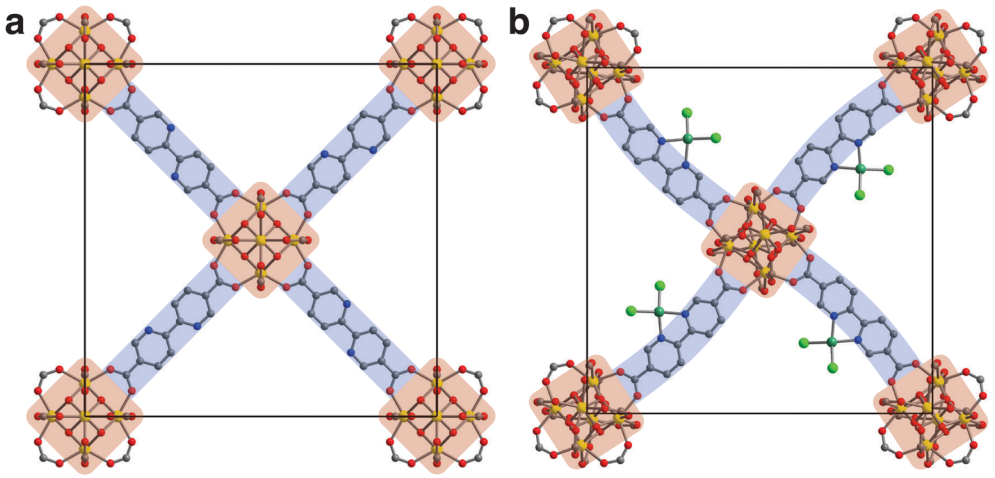

Figure 3. Comparison of the crystal structures of **1** (a) and **1**·$(CuCl_2)_{5.8}$ (b) viewed along the [100] direction; unit cell edges are shown as black lines. The bare framework exhibits mirror symmetry along the body diagonals of its unit cell and face-centering translations that relate the zirconium clusters at the ends of each linker. In the metalated structure, the mirror symmetry is removed by the ordering of the linkers, while the face-centering is lost because the clusters at the ends of each linker are tilted in opposite directions.

experimental powder pattern, indicating that the crystal structure is representative of the bulk material (Supporting Information Figure S9). As expected, the bipyridine units show disorder over two positions due to the $Fm\bar{3}m$ symmetry of the structure. While this Article was in preparation, similar results were reported from X-ray analysis of crystals of **1** grown under slightly different conditions.[40] Refinement of the linker occupancy in the structure revealed that 86% of the ligand was present, corresponding to the absence of roughly 1/6 of the linkers. When the ligand is not present, the vacancies on the cluster have been suggested to be occupied with water or hydroxide,[44−46] which can be identified as weak electron density peaks 2.18(4) Å away from Zr.

Metalation of $Zr_6O_4(OH)_4(bpydc)_6$. Transition metal halides were first considered for the metalation of **1**, as these were expected to form solvated metal species that would easily fit through the triangular windows of the framework, which have an incircle of ∼8 Å in diameter.[39] Soaking microcrystalline powders of **1** in acetonitrile solutions of metal halide salts (typically 1 equiv per bipyridine linker) at 80 °C for 5 days results in a color change (Table 1) of the powders over the course of the reaction. The powders remain colored after three acetonitrile washes at 80 °C, suggesting successful metalation of the framework. The powder X-ray diffraction patterns of the metalated frameworks **1**·$(CuCl_2)_{5.8}$, **1**·$(CuCl)_{6.8}$, **1**·$(CoCl_2)_{5.5}$, and **1**·$(FeBr_2)_{6.1}$ show additional peaks compared to that of **1**, indicating a possible change in space group upon metalation. Metal to zirconium ratios determined by ICP-OES analysis (Table 1) indicate a close to stoichiometric reaction of the bipyridine sites. Thermogravimetric analyses of the resulting powders generally showed slight decreases in thermal stability of the framework upon metalation (Supporting Information Figures S33−S38). This is likely due to weakened carboxylate−Zr bonds that result from less electron density being available to the linker carboxylate groups, as well as to strain induced by arching of the linker upon coordination of the linker bipyrdine moiety to a metal center, as discussed below.

Metal insertion in single crystals of **1** was carried out under the same conditions used for the bulk microcrystalline samples, with the exception of using excess metal precursor. Similar to the powders, the crystals change color with no visible loss in crystal quality after metalation. Analysis of the crystals by single-crystal X-ray diffraction revealed a lowering of the framework symmetry from $Fm\bar{3}m$ to $Pa\bar{3}$. Remarkably, the metalated bipyridine linkers were crystallographically ordered, allowing structural determination of the metal complexes formed within the framework (Figure 2).

Closer inspection of the structures shows that each bipyridine unit forms an arch to chelate the metal, presumably facilitating better orbital overlap with the metal (Figure 3). The zirconium clusters at the ends of each linker rotate slightly to accommodate the arching, while linkers around each cluster orient accordingly to conform to the direction of the cluster rotation. These distortions from the unmetalated structure collectively result in an ordering of the linker−metal complexes as they go from a site that has three mirror planes in $Fm\bar{3}m$ to a site with no symmetry in $Pa\bar{3}$.

Although there are several examples of the structural characterization of postsynthetically metalated metal−organic frameworks, most structures fail to resolve the complete ligand environment around the metal centers due to extensive disorder of the metalated linkers.[30,34,42] Recent work has emphasized that full characterization of metal-linkers complexes formed via postsynthetic metalation requires low symmetry at the location of the open chelating site in the crystal, which can be achieved by starting with a metal−organic framework with low crystal symmetry.[19] The crystallographic ordering of the linkers in **1** after postsynthetic metalation demonstrates that the structural characterization of the metalated linkers in high-symmetry metal−organic frameworks can be achieved if the framework has a pathway to lower symmetry during metalation. To the best of our knowledge, this is the first reported example of this phenomenon in a metal−organic framework.

X-ray analysis of **1**·$(CuCl_2)_{5.8}$ revealed significant ordering of both the framework and the acetonitrile molecules within the pores, which enabled reliable measurement of interatomic distances and angles for the (bpy)$CuCl_2$ units (Figure 2b). Interestingly, the Cu^{II} centers do not have acetonitrile bound, despite the presence of additional acetonitrile in the pores. The Cu−N distances of 1.993(4) and 2.007(4) Å and Cu−Cl distances of 2.2101(15) and 2.2126(16) Å in the complex were found to be very close to reported bond distances for the

DOI: 10.1021/acs.inorgchem.5b00096
Inorg. Chem. 2015, 54, 2995−3005

analogous molecular complex, $Cu(tbbpy)Cl_2$ (tbbpy = 4,4′-bis(*tert*-butyl)-2,2′-bipyridine).[47] The Cu^{II} centers exhibit a distorted square planar geometry, with the Cl−Cu−Cl plane tilted 33° away from the N−Cu−N plane, which is likely a result of steric repulsion between the Cl^- ligands and neighboring bipyridine H atoms. This distortion from planarity is common in molecular $(bpy)CuCl_2$ complexes and has been shown to vary with crystal packing.[47] While it was not possible to collect a single-crystal structure of activated $\mathbf{1}\cdot(CuCl_2)_{5.8}$, a structure was obtained from high-resolution powder X-ray diffraction data (Supporting Information Figure S16). In the activated structure, the Cu^{II} centers are in a similar coordination geometry, with the Cl−Cu−Cl plane tilted 45° away from the N−Cu−N plane.

Structural determination of the bipyridine metal complexes was more challenging for $\mathbf{1}\cdot(CuCl)_{6.8}$, $\mathbf{1}\cdot(CoCl_2)_{5.5}$, and $\mathbf{1}\cdot(FeBr_2)_{6.1}$, due to the disorder attributed to rotation of the linkers and variation in the degree of solvation of the metal complexes. The linkers in $\mathbf{1}\cdot(CuCl)_{6.8}$ show rotational disorder over two positions tilted 27° away from each other. Although the Cu^I complexes in $\mathbf{1}\cdot(CuCl)_{6.8}$ were modeled as distorted trigonal planar complexes with Cl^- as a coordinated counteranion (Figure 2c), residual electon density close to the Cu^I center suggests that 53% of the complexes actually have linear $[CuCl_2]^-$ units as a bound counteranion (Supporting Information Figure S1). Molecular complexes that are analogous to the (bpy)CuCl structural model exist.[48,49] The closest analogs to the $(bpy)Cu(CuCl_2)$ structural model contain phenanthroline- or bipyridine-Cu^I units bridged by $[CuCl_2]^-$ anions,[50,51] which cannot form in the framework due to the isolation of the bipyridine sites.

Similar to the structure of $\mathbf{1}\cdot(CuCl)_{6.8}$, the linkers in $\mathbf{1}\cdot(CoCl_2)_{5.5}$ displayed rotational disorder over two positions, tilted 14° away from each other. The bipyridine−$CoCl_2$ adducts were clearly located and appear to be square planar in one of the disordered positions (Figure 2d) and distorted square planar in the other (Supporting Information Figure S2). Residual electron density close to the Co^{II} centers, however, indicates that solvent is likely bound to Co^{II} and that the complexes are actually in octahedral and trigonal bipyramidal geometries (Supporting Information Figure S2), which are more consistent with published structures.[52,53] The square planar sites can be assigned to be octahedral with the bipyridine and Cl^- ligands coplanar and solvent on the axial sites, while the distorted square planar sites can be assigned as partially trigonal bipyramidal with the N and Cl on the axial sites and N, Cl, and solvent on the equatorial sites. Unfortunately, the disorder and weak scattering from the bound solvent molecules prevent a more accurate assignment of the Co^{II} complex geometries.

X-ray diffraction data for $\mathbf{1}\cdot(FeBr_2)_{6.1}$ collected on single crystals that were washed with acetonitrile alone gave structures with poorly resolved $FeBr_2$ moieties. The disorder in the structures can be attributed to the Fe^{II} complexes being in multiple states of solvation. Consequently, crystals were further washed with benzene at 80 °C in an attempt to fully desolvate the Fe^{II} centers. X-ray analysis of one of these crystals gives a much more ordered structure, with the Fe^{II} centers predominantly in a pseudotetrahedral geometry (Figure 2e), which is reasonable for $FeBr_2$ complexes with nitrogen-based chelating ligands.[54] Additional electron density peaks found near to the Fe^{II} centers suggests that a fraction of the complexes have the Br^- ligands closer to the Fe-bipyridine plane. Similar to $\mathbf{1}\cdot(CoCl_2)_{5.5}$, solvent may still be bound to on a fraction of the Fe^{II} sites, forcing them into what appears to be a pseodooctahedral geometry with the bipyridine and Br^- ligands on the equatorial sites and solvent on the axial sites (Supporting Information Figure S3). The geometry of these Fe^{II} sites, however, cannot be accurately assigned due to the disorder and the weak scattering from the coordinated solvent molecules on the Fe^{II} sites in comparison to the Br^- ligands.

Given the permanent porosity of **1**, we explored the possibility of using framework to chelate metals from reagents introduced in the gas phase. Heating a microcrystalline sample of **1** in a sealed vial with excess $Cr(CO)_6$ at 80 °C over 7 days results in gradual color change of the framework from white to dark green over the course of the reaction, consistent with the metalation of the bipyridine sites. Analysis of the resulting framework by infrared spectroscopy shows CO stretches at 2012, 1897, 1870, and 1845 cm^{-1} (Supporting Information Figure S43), consistent with the formation of $(bpy)Cr(CO)_4$ complexes within the framework.[55] Remarkably, single crystals of **1** can also be metalated and analyzed by X-ray diffraction, leading to structural confirmation that the complexes formed are indeed $(bpy)Cr(CO)_4$ (Figure 2f). These results emphasize the unique ability to perform and characterize gas phase reactions in metal−organic frameworks due to their inherent porosity and crystallinity.

The structures obtained for single crystals of $\mathbf{1}\cdot(Cr(CO)_4)_6$ from data collected directly after metalation show rotational disorder of the $(bpy)Cr(CO)_4$ units within the framework. Interestingly, soaking crystals of $\mathbf{1}\cdot(Cr(CO)_4)_6$ in acetonitrile results in ordering of the linkers, conceivably due to restriction of the rotational freedom of the linkers as the pores are filled with solvent. The Cr−N distances of 2.102(4) and 2.105(4) Å, equatorial Cr−C distances of 1.842(7) and 1.842(7) Å, and equatorial C−O distances of 1.173(8) and 1.167(9) Å are all in good agreement with analogous complexes in the literature.[56] In contrast, the axial Cr−C distances of 1.77(1) and 1.78(2) Å and C−O distances of 1.29(2) and 1.24(2) Å are comparatively shorter, which may be an artifact of slight disorder of the $(bpy)Cr(CO)_4$ complexes along the direction of these bonds.

Gas Adsorption. Low-pressure N_2 adsorption data (Supporting Information Figure S17) collected at 77 K for metalated frameworks reveal a considerable decrease in surface area upon metalation of **1** (Table 1). These results are consistent with loss of accessible pore surface due to the metal-linker complexes occupying additional space in the pores. In line with this, frameworks with bulkier metal complexes exhibit lower surface areas, with the exception of $\mathbf{1}\cdot(CuCl)_{6.8}$. The low surface area of $\mathbf{1}\cdot(CuCl)_{6.8}$ relative to the other metal halide metalated frameworks may be attributed to some of the Cu sites in $\mathbf{1}\cdot(CuCl)_{6.8}$ possessing the much larger $[CuCl_2]^-$ as a counteranion instead of the Cl^-.

To determine the accessibility of the metal sites in $\mathbf{1}\cdot(CuCl_2)_{5.8}$, $\mathbf{1}\cdot(CuCl)_{6.8}$, $\mathbf{1}\cdot(CoCl_2)_{5.5}$, $\mathbf{1}\cdot(FeBr_2)_{6.1}$, and $\mathbf{1}\cdot(Cr(CO)_4)_{5.6}$, low-pressure H_2 adsorption measurements were performed at 77 K (Figure 4). All metalated frameworks except $\mathbf{1}\cdot(CuCl)_{6.8}$ displayed improved gravimetric H_2 uptake over the bare framework at low pressures, despite their lower surface areas and increased formula weights. The isotherms, however, did not show any steep uptake at very low pressures characteristic of strong interaction with open metal sites.[57] Instead, the increased H_2 capacity likely arises from the introduction of additional weakly polarizing sites and the formation of tighter binding pockets within the pores of the

DOI: 10.1021/acs.inorgchem.5b00096
Inorg. Chem. 2015, 54, 2995−3005

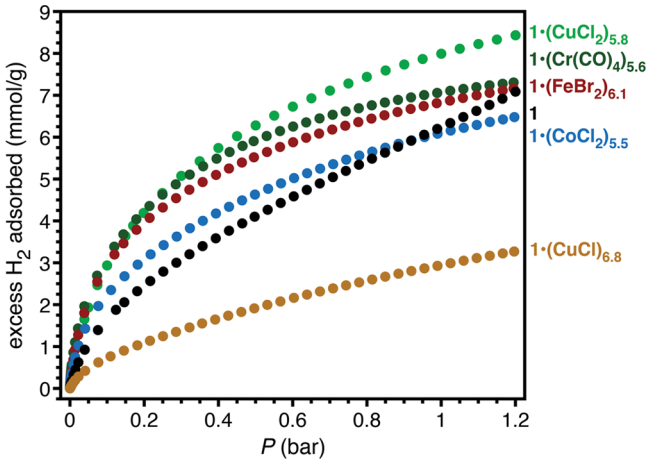

Figure 4. Low-pressure H_2 adsorption isotherms for **1**, **1**·$(CuCl_2)_{5.8}$, **1**·$(CuCl)_{6.8}$, **1**·$(CoCl_2)_{5.5}$, **1**·$(FeBr_2)_{6.1}$, and **1**·$(Cr(CO)_4)_{5.6}$ at 77 K.

framework. Similar results have been reported for CO_2 adsorption in metalated samples of another bipyridine-containing framework, Al(OH)(bpydc).[38]

Although there is ample space in the coordination sphere of the metal-linker complexes in **1**·$(CuCl_2)_{5.8}$ and **1**·$(CuCl)_{6.8}$, these metal centers only show weak interaction with additional ligands, preferring lower coordination as a result of their filled d shells. While the Co^{II} and Fe^{II} centers in **1**·$(CoCl_2)_{5.5}$ and **1**·$(FeBr_2)_{6.1}$ should be able to achieve higher coordination, these complexes have the propensity to form tetrahedral complexes after desolvation. Weakly coordinating gases such as H_2 cannot bind to these metal centers, most likely because the resulting binding energy would not compensate for the reorganization energy required for conversion to geometries that support a higher coordination number.

Carbon monoxide adsorption experiments were performed on **1**·$(CuCl_2)_{5.8}$, **1**·$(CuCl)_{6.8}$, **1**·$(CoCl_2)_{5.5}$, and **1**·$(FeBr_2)_{6.1}$ at 298 K to probe the interaction of the metal sites with a more coordinating gas (Figure 5). Surprisingly, only **1**·$(CuCl)_{6.8}$ showed significant uptake of CO, reaching a level of approximately 0.4 per copper center at 0.2 bar. Here, coordination of CO to the Cu^I centers is confirmed by the observation of a peak at 2093 cm^{-1} in the infrared spectrum, which agrees with reported CO stretching frequencies in similar

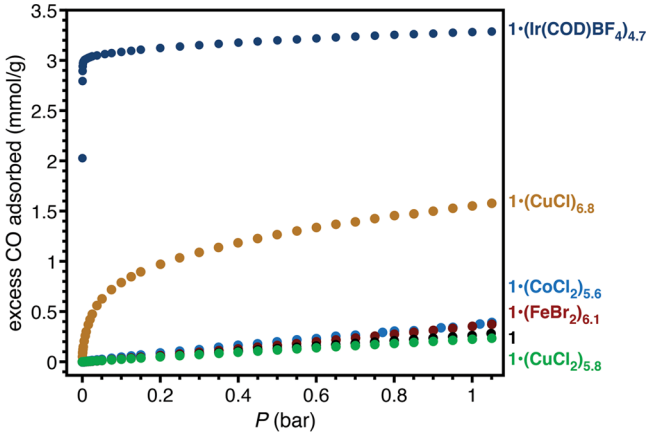

Figure 5. Low-pressure CO adsorption isotherms for **1**, **1**·$(CuCl_2)_{5.8}$, **1**·$(CuCl)_{6.8}$, **1**·$(CoCl_2)_{5.5}$, **1**·$(FeBr_2)_{6.1}$ and **1**·$(Ir(COD)BF_4)_{4.8}$ at 298 K.

molecular Cu^I–CO complexes (Supporting Information Figure S42).[58] The CO stretching frequency in the CO adduct of **1**·$(CuCl)_{6.8}$ is shifted 50 cm^{-1} lower relative to free CO, indicating modest π backbonding from Cu^I to CO. Substoichiometric uptake of CO per Cu^I suggests that CO binds to only one type of Cu^I center among the three determined in the single-crystal structure (Supporting Information Figure S1). In contrast, the lack of any strong interaction between CO and **1**·$(CuCl_2)_{5.8}$, **1**·$(CoCl_2)_{5.5}$, or **1**·$(FeBr_2)_{6.1}$ suggests that the metal centers in these materials have insufficient π backbonding capability to form stable adducts with CO, which is attributed to the higher formal oxidation state of the metal centers in the bipyridine-M^{II} complexes.

Arene C–H Borylation. Iridium-catalyzed C–H borylation has proven to be a practical and efficient way of functionalizing inert feedstock chemicals to make valuable products that are widely used in fine chemicals synthesis.[59] Among the many catalysts studied for this reaction, iridium complexes supported by chelating N-donor ligands have been shown to be very capable systems for the C–H borylation of arenes with either 4,4,4′,4′,5,5,5′,5′-octamethyl-2,2′-bi-1,3,2-dioxaborolane (B_2pin_2) or 4,4,5,5-tetramethyl-1,3,2-dioxaborolane (HBpin).[60−63] Inspired by the considerable amount of work on homogeneous systems, recent efforts have been directed toward making heterogeneous analogs of these catalysts.[33,64,65] Given that Ir^I precursors in combination with 2,2′-bipyrdine ligands lead to highly active homogeneous systems, we investigated whether **1** would show similar activity when metalated with iridium.

Considering the size of the pore apertures in **1**, $[Ir(COD)_2]$-BF_4 (COD = 1,5-cyclooctadiene) was selected as an metalation agent, as it forms a relatively compact complex, $[Ir(COD)(MeCN)_2]^+$, in acetonitrile.[66] Metalation of a microcrystalline powder of **1** with $[Ir(COD)_2]BF_4$ following the procedure used for the metal halides indeed yields **1**·$(Ir(COD)BF_4)_{4.7}$ as an olive green powder. ICP-OES analysis of the powder indicates 78% Ir loading of the framework, which is much lower than the loading determined for the frameworks metalated with first-row transition metal halides. X-ray analysis of the metalated single crystals revealed no change in space group and less than 10% occupancy of Ir at the bipyridine sites. Consequently, the ancillary ligands on Ir could not be identified. Disparity between the Ir loading in the powder and single-crystal samples implies that the extent of metalation at the framework surface is greater than that of the interior. Compared to ∼60 μm single crystals, the ∼0.5−1 μm crystals in the powder sample have a much larger crystal surface area to volume ratio, which would result in higher Ir loading in the powder. The Ir source may be blocking the pore windows upon metalation, obstructing the diffusion of additional Ir complexes to sites within the framework. This may be due to the larger size of the Ir precursor compared to the first row transition metal halides. In addition, Ir forms much more stable complexes with bipyrdine, making it less likely to reversibly dissociate from the bipyridine sites and travel deeper into the pore structure.

To provide insight into the structure of the Ir centers formed in **1**·$(Ir(COD)BF_4)_{4.7}$, CO adsorption measurements were performed. These indicate substantial irreversible binding of CO with uptake of roughly two CO molecules per Ir center by 0.001 bar CO. This presumably occurs through the substitution of CO for COD on the Ir center to form **1**·$(Ir(CO)_2BF_4)_{4.7}$. After CO adsorption, the resulting yellow material features two

DOI: 10.1021/acs.inorgchem.5b00096
Inorg. Chem. 2015, 54, 2995−3005

new peaks in the infrared spectrum at 2088 and 2026 cm^{-1} (Supporting Information Figure S41), which can be assigned to the asymmetric and symmetric CO stretching modes of the $(bpy)Ir(CO)_2$ complex. These frequencies agree with those reported for similar cationic Ir^I dicarbonyl complexes.[67,68]

The compound $[Ir(dmbpydc)(COD)]BF_4$ (**3**) was also synthesized as a molecular analog and characterized by single-crystal X-ray diffraction. The structure of **3** (see Figure 6)

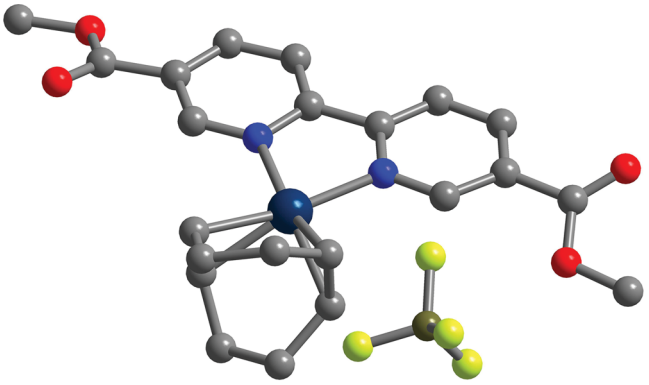

Figure 6. Crystal structure of **3**, the molecular analog of **1**·$(Ir(COD)BF_4)_{4.7}$ as determined by single-crystal X-ray diffraction. Dark blue, yellow green, olive green, red, blue, and gray spheres represent Ir^I, F, B, O, N, and C atoms, respectively; H atoms are omitted for clarity.

supports the initial description of the Ir complexes in **1**·$(Ir(COD)BF_4)_{4.7}$, with dmbpydc and COD bound to Ir in a square planar geometry and BF_4^- as a noncoordinating anion. The UV–vis spectrum of **1**·$(Ir(COD)BF_4)_{4.7}$ (Supporting Information Figure S44) reveals a shoulder at 466 nm and a peak at 594 nm, which likely correspond to the metal-to-ligand charge transfer bands of the Ir-bpy units in the framework. These correspond well to peaks at 466 and 602 nm in the UV–vis spectrum of **3**. Furthermore, infrared spectra of **1**·$(Ir(COD)BF_4)_{4.7}$ (Supporting Information Figure S41) exhibits peaks between 2922 and 2841 cm^{-1}, which are assigned to the aliphatic ν(C–H) of the coordinated COD moieties, and a broad peak at 1056 cm^{-1}, which is assigned to ν(B–F) of the BF_4^- anion. Both features can also be observed in the same regions in the infrared spectrum of **3**. These results suggest that the structure of **3** is representative of the Ir-bipyridine complexes in **1**·$(Ir(COD)BF_4)_{4.7}$.

Borylation reactions were generally conducted over 24 h at 80 °C in neat arene using either B_2pin_2 or HBpin as a boron reagent. To ensure that the Ir sites in the framework are accessible and to achieve catalyst loadings below 1 mol % Ir, only 10% of the bipyridine sites were metalated in the samples employed for catalysis. The Ir-metalated framework, **1**·$(Ir(COD)BF_4)_{0.6}$, proved to be a highly active catalyst for the C–H borylation of benzene to form 4,4,5,5-tetramethyl-2-phenyl-1,3,2-dioxaborolane (PhBpin) in good yield at a very low catalyst loading (Tables 2 and 3). Comparison of the powder X-ray diffraction patterns of the material before and after catalysis reveals no loss in crystallinity, suggesting that the material is stable under the conditions used for catalysis. Following conversion of benzene to PhBpin by ^1H NMR spectroscopy, the average turnover frequency of the catalyst was determined to be 860 mol PhBpin mol Ir^{-1} h^{-1} at 80 °C (Supporting Information Figure S45), which is within an order

Table 2. Control Experiments for Benzene C–H Borylation with HBpin

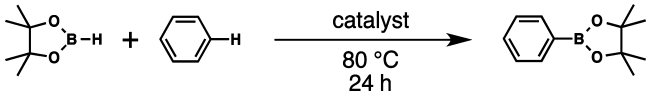

catalyst	amount (mol %)	yield[a] (%)
1·$(Ir(COD)(BF_4))_{0.6}$	0.065 (Ir)	100[b]
1	0.68 (Zr)	0
$[Ir(COD)_2]BF_4$	0.18 (Ir)	0.9
2 + 0.6$[Ir(COD)_2]BF_4$	0.84 (Zr)	0.03
1·$(Ir(COD)(BF_4))_{0.6}$ + 0.6PPh_3	0.065 (Ir)	4
1·$(Ir(COD)(BF_4))_{0.6}$ + 0.6PCy_3	0.069 (Ir)	4

[a]Yields were determined by ^1H NMR using 1,3,5-trimethoxybenzene as an internal standard. [b]Determined as an average of three replications.

Table 3. Control Experiments for Benzene C–H Borylation with B_2pin_2

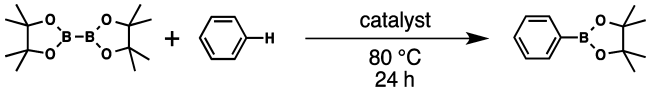

catalyst	amount (mol %)	yield[a] (%)
1·$(Ir(COD)(BF_4))_{0.6}$	0.21 (Ir)	94[b]
1	2.4 (Zr)	0
$[Ir(COD)_2]BF_4$	0.71 (Ir)	0.9
2 + 0.6$[Ir(COD)_2]BF_4$	2.3 (Zr)	0
1·$(Ir(COD)(BF_4))_{0.6}$ + 0.6PPh_3	0.21 (Ir)	0.05
1·$(Ir(COD)(BF_4))_{0.6}$ + 0.6PCy_3	0.20 (Ir)	0

[a]Yields were determined by ^1H NMR spectroscopy using 1,3,5-trimethoxybenzene as an internal standard. [b]Determined as an average of three replications.

of magnitude of that reported for the best molecular systems.[61] Note that supporting ligands that are stronger electron donors are better at stabilizing the proposed Ir^V intermediate that forms upon C–H activation of the arene,[59,61,63] which is often the rate-determining step of the reaction. Thus, the bipyridine-Ir units in **1**·$(Ir(COD)BF_4)_{0.6}$ are expected to be less active in comparison to the best molecular Ir catalysts with more electron-rich supporting ligands, such as 4,4′-di-*tert*-butylbipyridine or 3,4,7,8-tetramethylphenanthroline.[61,63]

Several control experiments were performed to establish that catalysis is indeed facilitated by the Ir-bipyridine complexes in framework (Tables 2 and 3). As predicted, $[Ir(COD)_2]BF_4$ and **1** both display limited or no catalytic activity. The metal–organic framework $Zr_6O_4(OH)_4(bpdc)_6$ was synthesized and treated with $[Ir(COD)_2]BF_4$ following the same procedure used for **1**. The Ir-treated biphenyl framework did not show significant catalytic activity, excluding the possibility of catalysis by adventitious Ir species that may form upon interaction with the framework. A hot filtration experiment was performed to determine if any catalytic activity was due to soluble Ir species that may have formed during the reaction. No further increase in turnover number was observed after **1**·$(Ir(COD)BF_4)_{0.6}$ was filtered from the reaction mixture (Supporting Information Figure S46), which further supports that catalysis is facilitated by the Ir-bipyridine complexes bound within the material.

To determine if catalysis occurs within the pores or only on the surface of the metal–organic framework crystallites, reactions were carried out in the presence of bulky coordinating groups, which can selectively poison the surface Ir sites due to

DOI: 10.1021/acs.inorgchem.5b00096
Inorg. Chem. 2015, 54, 2995–3005

their large size (Table 3).[66] Addition of 1 equiv of either PPh_3 or PCy_3 per Ir to the reaction mixture led to drastically reduced yields, suggesting that catalysis occurs primarily at the surface of the material. This is consistent with Ir binding to only surface bipyrdine sites and not to those within the pores.

Catalyst cycling experiments indicated no significant loss in activity over five cycles when HBpin was employed, although activity decreased substantially after the third and fourth cycles when B_2pin_2 was used (Table 4). The much lower catalyst

Table 4. Catalyst Cycling Experiments for Benzene C−H Borylation with $Zr_6O_4(OH)_4(bpydc)_6(Ir(COD)BF_4)_{0.6}$

	yield[a] (%)				
boron reagent	1	2	3	4	5
HBpin[b]	96	100	100	100	96
B_2pin_2[c]	94	91	90	80	54

[a]Yields were determined by ^{1}H NMR using 1,3,5-trimethoxybenzene as an internal standard. [b]Reaction conditions: 1.3 mmol HBpin, 3.0 mL benzene, 0.10 mol % Ir, 80 °C, 24 h. [c]Reaction conditions: 0.65 mmol B_2pin_2, 3.0 mL benzene, 0.20 mol % Ir, 80 °C, 24 h.

stability with B_2pin_2 may be attributed to impurities such as trace moisture in the B_2pin_2 that can poison the catalytic sites. It has previously been reported that the maximum turnover number of the catalyst is highly dependent on the purity of the B_2pin_2 used.[60,61] If the catalyst were inherently unstable to the reaction conditions, decreased activity after each cycle should have also been observed when HBpin was used as a boron reagent.

The activity of $\mathbf{1}\cdot(Ir(COD)(BF_4))_{0.6}$ in the borylation of several substituted arenes reveals that the catalyst exhibits size selectivity. Reaction with toluene, or 1,2-difluorobenzene, results in nearly quantitative borylation, whereas substantially lower activity is observed using *tert*-butylbenzene, *o*-xylene, and *m*-xylene as substrates (Table 5). Assuming that the catalytic sites are predominantly on the surface, as suggested by surface poisoning experiments and low Ir loading after metalation, the unexpected size selectivity suggests that the local steric environment of the catalytic sites on the framework surface can prevent access to the Ir centers or destabilize ideal transition state conformations when bulkier substrates are used. A substrate competition experiment between benzene and *m*-xylene in 1:1 mixture showed that the catalyst has 95% selectivity for benzene, further suggesting that the lower yields observed for bulkier arenes are due to size or shape selectivity and not catalyst instability or poisoning from trace impurities in these solvents. Although size selectivity is not necessarily ideal for this specific reaction, which has applications that require the ability to functionalize a broad scope of substrates, it is intriguing to observe that size selectivity still occurs even if the catalytic sites are likely on the surface of the particles. This implies that size selectivity in metal−organic frameworks does not have to arise solely from restriction of substrate access to catalytic sites by the pore apertures, but can also be influenced by the local steric environment around the catalytic sites, as dictated by the unique pore structure of a specific framework.

While this Article was in preparation, a recent paper reported the similar application of $Zr_6O_4(OH)_4(bpydc)_6$ using $[Ir(COD)(OMe)]_2$ as an Ir source and B_2pin_2 as the boron source.[33] Interestingly, the catalyst described in the report maintained activity after 20 cycles using B_2pin_2 and displayed no pronounced size selectivity. The disparity between the

Table 5. Selected Substrate Scope for C−H Borylation with HBpin[a]

Substrates	Products	Product Ratio[b]	Conversion[b] (%)
		–	100[c]
	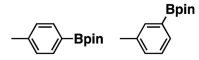	40:60	96
	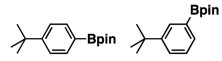	29:71	38
	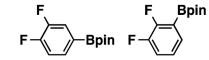	67:33	96
	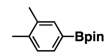	–	4
		–	27
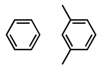 1:1	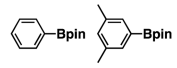	95:5	97

[a]Reaction conditions: 2.0 mmol HBpin, 3 mL arene or arene mixture, 0.065 mol % Ir, 80 °C, 24 h. [b]Product ratios and conversions were determined by ^{1}H NMR using 1,3,5-trimethoxybenzene as an internal standard. [c]Determined as an average of three replications.

reported results and the results in this work may be due to differences in particle size, surface morphology, and metal loading of the material, which indicates that these properties may have unexpected and profound effects on catalysis and, thus, should be more carefully studied.

CONCLUSIONS AND OUTLOOK

The foregoing results demonstrate that $Zr_6O_4(OH)_4(bpydc)_6$, a metal−organic framework featuring open 2,2′-bipyridine sites, can readily be metalated by a host of solution- and gas-phase metal reagents. Moreover, single-crystal-to-single-crystal metalation of the framework results in the ordering of the metal-linker complexes, enabling structural characterization by single-crystal X-ray diffraction. This remarkable structural ordering arises from a transition from $Fm\bar{3}m$ to $Pa\bar{3}$ symmetry induced by the collective distortion of the framework linkers upon metal chelation. These findings emphasize that structural determination of the metal complexes in postsynthetically metalated metal−organic frameworks can be achieved if a high-symmetry framework can transition to a lower symmetry upon metal insertion. Furthermore, the $[Ir(COD)_2]BF_4$-metalated framework is a highly active and recyclable catalyst for arene C−H borylation.

Ongoing efforts are directed toward finding other frameworks that display similar structural transitions upon metalation, as well as to developing methods to limit disorder due to linker rotation and variable solvation of the metal. In addition, the *in situ* structural observation of reactions at the metal sites in these frameworks by X-ray diffraction is being pursued. Finally, efforts are underway to demonstrate that postsynthetic metalation of metal−organic frameworks can be used to design catalysts with unparalleled reactivity and selectivity through judicious choice of metal node, chelating linker, and metal precursor. Altogether, these results exemplify the distinct advantages that metal−organic frameworks hold as highly tunable, well-defined platforms for catalysis and the exceptional

DOI: 10.1021/acs.inorgchem.5b00096
Inorg. Chem. 2015, 54, 2995−3005

ability to structurally characterize these materials through X-ray diffraction.

■ ASSOCIATED CONTENT

Supporting Information

Additional experimental procedures and structural, powder X-ray diffraction, gas adsorption, thermogravimetric analysis, and catalysis data. Crystallographic data in CIF format. This material is available free of charge via the Internet at http://pubs.acs.org.

■ AUTHOR INFORMATION

Corresponding Author

*E-mail: jrlong@berkeley.edu.

Present Address

For E.D.B.: Department of Chemistry and Chemical Biology, Harvard University, 12 Oxford Street, Cambridge, Massachusetts 02138, United States.

Notes

The authors declare no competing financial interest.

■ ACKNOWLEDGMENTS

This work was supported by the Laboratory Directed Research and Development Program of Lawrence Berkeley National Laboratory under U.S. Department of Energy Contract DE-AC02-05CH11231. The Advanced Light Source is supported by the Director, Office of Science, Office of Basic Energy Sciences, of the U.S. Department of Energy under Contract DE-AC02-05CH11231. We thank the 11-BM staff at the Advanced Photon Source at Argonne National Laboratory for assisting with powder X-ray diffraction experiments. Use of the Advanced Photon Source at Argonne National Laboratory was supported by the U.S. Department of Energy, Office of Science, Office of Basic Energy Sciences, under Contract DE-AC02-06CH11357. We thank Gerald K. Branch and Arkema for the fellowship support of E.D.B and Chevron for fellowship support of J.A.M. We are grateful for the assistance of Antonio DiPasquale and Kevin J. Gagnon with single-crystal X-ray diffraction experiments and Jonathan Bachman with SEM measurements. We also thank Kohei Takahashi, Matthew Larsen, and Carl Liskey for fruitful discussions.

■ REFERENCES

(1) Serna, P.; Gates, B. C. *Acc. Chem. Res.* **2014**, *47*, 2612−2620.
(2) Wegener, S. L.; Marks, T. J.; Stair, P. C. *Acc. Chem. Res.* **2012**, *45*, 206−214.
(3) Hagen, J. *Industrial Catalysis*; John Wiley & Sons: New York, 2006.
(4) Furukawa, H.; Ko, N.; Go, Y. B.; Aratani, N.; Choi, S. B.; Choi, E.; Yazaydin, A. O.; Snurr, R. Q.; O'Keeffe, M.; Kim, J.; Yaghi, O. M. *Science* **2010**, *329*, 424−428.
(5) Eddaoudi, M.; Kim, J.; Rosi, N.; Vodak, D.; Wachter, J.; O'Keeffe, M.; Yaghi, O. M. *Science* **2002**, *295*, 469−472.
(6) Cohen, S. M. *Chem. Rev.* **2012**, *112*, 970−1000.
(7) Murray, L. J.; Dincă, M.; Long, J. R. *Chem. Soc. Rev.* **2009**, *38*, 1294−1314.
(8) Sumida, K.; Rogow, D. L.; Mason, J. A.; McDonald, T. M.; Bloch, E. D.; Herm, Z. R.; Bae, T.-H.; Long, J. R. *Chem. Rev.* **2012**, *112*, 724−781.
(9) Herm, Z. R.; Bloch, E. D.; Long, J. R. *Chem. Mater.* **2014**, *26*, 323−338.
(10) Mason, J. A.; Veenstra, M.; Long, J. R. *Chem. Sci.* **2013**, *5*, 32−51.
(11) Corma, A.; García, H.; Llabrés, i; Xamena, F. X. *Chem. Rev.* **2010**, *110*, 4606−4655.
(12) Wang, C.; Zheng, M.; Lin, W. *J. Phys. Chem. Lett.* **2011**, *2*, 1701−1709.
(13) Ma, L.; Abney, C.; Lin, W. *Chem. Soc. Rev.* **2009**, *38*, 1248.
(14) Xiao, D. J.; Bloch, E. D.; Mason, J. A.; Queen, W. L.; Hudson, M. R.; Planas, N.; Borycz, J.; Dzubak, A. L.; Verma, P.; Lee, K.; Bonino, F.; Crocellà, V.; Yano, J.; Bordiga, S.; Truhlar, D. G.; Gagliardi, L.; Brown, C. M.; Long, J. R. *Nat. Chem.* **2014**, *6*, 590−595.
(15) Pullen, S.; Fei, H.; Orthaber, A.; Cohen, S. M.; Ott, S. *J. Am. Chem. Soc.* **2013**, *135*, 16997−17003.
(16) Fei, H.; Shin, J.; Meng, Y. S.; Adelhardt, M.; Sutter, J.; Meyer, K.; Cohen, S. M. *J. Am. Chem. Soc.* **2014**, *136*, 4965−4973.
(17) Feng, D.; Gu, Z.-Y.; Li, J.-R.; Jiang, H.-L.; Wei, Z.; Zhou, H.-C. *Angew. Chem., Int. Ed.* **2012**, *51*, 10307−10310.
(18) Anderson, J. S.; Gallagher, A. T.; Mason, J. A.; Harris, T. D. *J. Am. Chem. Soc.* **2014**, *136*, 16489−16492.
(19) Bloch, W. M.; Burgun, A.; Coghlan, C. J.; Lee, R.; Coote, M. L.; Doonan, C. J.; Sumby, C. J. *Nat. Chem.* **2014**, *6*, 906−912.
(20) Dhakshinamoorthy, A.; Alvaro, M.; Garcia, H. *Catal. Sci. Technol.* **2011**, *1*, 856.
(21) Dhakshinamoorthy, A.; Alvaro, M.; Garcia, H. *Chem. Commun.* **2012**, *48*, 11275.
(22) Dhakshinamoorthy, A.; Opanasenko, M.; Čejka, J.; Garcia, H. *Catal. Sci. Technol.* **2013**, *3*, 2509.
(23) Horike, S.; Dincă, M.; Tamaki, K.; Long, J. R. *J. Am. Chem. Soc.* **2008**, *130*, 5854−5855.
(24) Juan-Alcañiz, J.; Gascon, J.; Kapteijn, F. *J. Mater. Chem.* **2012**, *22*, 10102.
(25) Genna, D. T.; Wong-Foy, A. G.; Matzger, A. J.; Sanford, M. S. *J. Am. Chem. Soc.* **2013**, *135*, 10586−10589.
(26) Meilikhov, M.; Yusenko, K.; Esken, D.; Turner, S.; Van Tendeloo, G.; Fischer, R. A. *Eur. J. Inorg. Chem.* **2010**, *2010*, 3701−3714.
(27) Li, L.; Matsuda, R.; Tanaka, I.; Sato, H.; Kanoo, P.; Jeon, H. J.; Foo, M. L.; Wakamiya, A.; Murata, Y.; Kitagawa, S. *J. Am. Chem. Soc.* **2014**, *136*, 7543−7546.
(28) Hasegawa, S.; Horike, S.; Matsuda, R.; Furukawa, S.; Mochizuki, K.; Kinoshita, Y.; Kitagawa, S. *J. Am. Chem. Soc.* **2007**, *129*, 2607−2614.
(29) Wang, C.; Xie, Z.; deKrafft, K. E.; Lin, W. *J. Am. Chem. Soc.* **2011**, *133*, 13445−13454.
(30) Wang, C.; deKrafft, K. E.; Lin, W. *J. Am. Chem. Soc.* **2012**, *134*, 7211−7214.
(31) Dau, P. V.; Cohen, S. M. *Chem. Commun.* **2013**, *49*, 6128.
(32) Fei, H.; Cohen, S. M. *Chem. Commun.* **2014**, *50*, 4810−4812.
(33) Manna, K.; Zhang, T.; Lin, W. *J. Am. Chem. Soc.* **2014**, *136*, 6566−6569.
(34) Falkowski, J. M.; Sawano, T.; Zhang, T.; Tsun, G.; Chen, Y.; Lockard, J. V.; Lin, W. *J. Am. Chem. Soc.* **2014**, *136*, 5213−5216.
(35) Manna, K.; Zhang, T.; Carboni, M.; Abney, C. W.; Lin, W. *J. Am. Chem. Soc.* **2014**, *136*, 13182−13185.
(36) Valvekens, P.; Bloch, E. D.; Long, J. R.; Ameloot, R.; De Vos, D. E. *Catal. Today* **2014**, *246*, 55.
(37) Evans, J. D.; Sumby, C. J.; Doonan, C. J. *Chem. Soc. Rev.* **2014**, *43*, 5933−5951.
(38) Bloch, E. D.; Britt, D.; Lee, C.; Doonan, C. J.; Uribe-Romo, F. J.; Furukawa, H.; Long, J. R.; Yaghi, O. M. *J. Am. Chem. Soc.* **2010**, *132*, 14382−14384.
(39) Cavka, J. H.; Jakobsen, S.; Olsbye, U.; Guillou, N.; Lamberti, C.; Bordiga, S.; Lillerud, K. P. *J. Am. Chem. Soc.* **2008**, *130*, 13850−13851.
(40) Li, L.; Tang, S.; Wang, C.; Lv, X.; Jiang, M.; Wu, H.; Zhao, X. *Chem. Commun.* **2014**, *50*, 2304−2307.
(41) Nickerl, G.; Leistner, M.; Helten, S.; Bon, V.; Senkovska, I.; Kaskel, S. *Inorg. Chem. Front.* **2014**, *1*, 325−330.
(42) Dau, P. V.; Kim, M.; Cohen, S. M. *Chem. Sci.* **2013**, *4*, 601.
(43) Schaate, A.; Roy, P.; Godt, A.; Lippke, J.; Waltz, F.; Wiebcke, M.; Behrens, P. *Chem.—Eur. J.* **2011**, *17*, 6643−6651.

DOI: 10.1021/acs.inorgchem.5b00096
Inorg. Chem. 2015, 54, 2995−3005

(44) Valenzano, L.; Civalleri, B.; Chavan, S.; Bordiga, S.; Nilsen, M. H.; Jakobsen, S.; Lillerud, K. P.; Lamberti, C. *Chem. Mater.* **2011**, *23*, 1700−1718.
(45) Katz, M. J.; Brown, Z. J.; Colón, Y. J.; Siu, P. W.; Scheidt, K. A.; Snurr, R. Q.; Hupp, J. T.; Farha, O. K. *Chem. Commun.* **2013**, *49*, 9449.
(46) Shearer, G. C.; Chavan, S.; Ethiraj, J.; Vitillo, J. G.; Svelle, S.; Olsbye, U.; Lamberti, C.; Bordiga, S.; Lillerud, K. P. *Chem. Mater.* **2014**, *26*, 4068−4071.
(47) Awad, D. J.; Schilde, U.; Strauch, P. *Inorg. Chim. Acta* **2011**, *365*, 127−132.
(48) Healy, P. C.; Pakawatchai, C.; White, A. H. *J. Chem. Soc., Dalton Trans.* **1985**, 2531−2539.
(49) Hong, J.; Li, X.-Y.; Ng, S. W. *Acta Crystallogr., Sect. E* **2011**, *67*, M1322−U1496.
(50) Xiao, L. N.; Wang, Y.; Pan, C. L.; Xu, J. N.; Wang, T. G.; Ding, H. *CrystEngComm* **2011**, *13*, 4878.
(51) Cui, Y.; Chen, J.; Chen, G.; Ren, J.; Yu, W.; Qian, Y. *Acta Crystallogr., Sect. C* **2001**, *57*, 349−351.
(52) Desroches, C.; Ohrström, L. *Acta Crystallogr., Sect. C* **2007**, *63*, m190−m192.
(53) Brewer, B.; Brooks, N. R.; Sykes, A. G. *J. Chem. Crystallogr.* **2003**, *33*, 663−668.
(54) Volbeda, J.; Meetsma, A.; Bouwkamp, M. W. *Organometallics* **2009**, *28*, 209−215.
(55) Vlcek, A.; Grevels, F. W.; Snoeck, T. L.; Stufkens, D. J. *Inorg. Chim. Acta* **1998**, *278*, 83−90.
(56) Baxter, P. N. W.; Connor, J. A.; Wallis, J. D.; Povey, D. C.; Powell, A. K. *Polyhedron* **1992**, *11*, 1771−1777.
(57) Zhou, W.; Wu, H.; Yildirim, T. *J. Am. Chem. Soc.* **2008**, *130*, 15268−15269.
(58) Ugozzoli, F.; Lanfredi, A. M. M.; Marsich, N.; Camus, A. *Inorg. Chim. Acta* **1997**, *256*, 1−7.
(59) Mkhalid, I. A. I.; Barnard, J. H.; Marder, T. B.; Murphy, J. M.; Hartwig, J. F. *Chem. Rev.* **2010**, *110*, 890−931.
(60) Ishiyama, T.; Takagi, J.; Ishida, K.; Miyaura, N.; Anastasi, N. R.; Hartwig, J. F. *J. Am. Chem. Soc.* **2002**, *124*, 390−391.
(61) Boller, T. M.; Murphy, J. M.; Hapke, M.; Ishiyama, T.; Miyaura, N.; Hartwig, J. F. *J. Am. Chem. Soc.* **2005**, *127*, 14263−14278.
(62) Tajuddin, H.; Harrisson, P.; Bitterlich, B.; Collings, J. C.; Sim, N.; Batsanov, A. S.; Cheung, M. S.; Kawamorita, S.; Maxwell, A. C.; Shukla, L.; Morris, J.; Lin, Z.; Marder, T. B.; Steel, P. G. *Chem. Sci.* **2012**, *3*, 3505.
(63) Larsen, M. A.; Hartwig, J. F. *J. Am. Chem. Soc.* **2014**, *136*, 4287−4299.
(64) Waki, M.; Maegawa, Y.; Hara, K.; Goto, Y.; Shirai, S.; Yamada, Y.; Mizoshita, N.; Tani, T.; Chun, W.-J.; Muratsugu, S.; Tada, M.; Fukuoka, A.; Inagaki, S. *J. Am. Chem. Soc.* **2014**, *136*, 4003−4011.
(65) Wu, F.; Feng, Y.; Jones, C. W. *ACS Catal.* **2014**, 1365−1375.
(66) Green, M.; Kuc, T. A.; Taylor, S. H. *J. Chem. Soc., A* **1971**, 2334−2337.
(67) Rahaman, S. M. W.; Dinda, S.; Ghatak, T.; Bera, J. K. *Organometallics* **2012**, *31*, 5533−5540.
(68) Harding, D. A. J.; Hope, E. G.; Singh, K.; Solan, G. A. *Polyhedron* **2012**, *33*, 360−366.

■ NOTE ADDED AFTER ASAP PUBLICATION

This paper was published ASAP on February 26, 2015. Additional Supporting Information was posted on the Web on February 27, 2015.

DOI: 10.1021/acs.inorgchem.5b00096
Inorg. Chem. 2015, 54, 2995−3005